Solar Energy Materials & Solar Cells 230 (2021) 111208

Contents lists available at ScienceDirect

Solar Energy Materials and Solar Cells

journal homepage: www.elsevier.com/locate/solmat

Fast and accurate short-circuit current versus irradiance determination of a spectrally nonlinear solar cell using a spectral shaping setup

Matthias Mühleis [a,*], Ingo Kröger [b], Jochen Hohl-Ebinger [a]

[a] Fraunhofer Institute for Solar Energy Systems ISE, Heidenhofstrasse 2, Freiburg, 79110, Germany
[b] Physikalisch-Technische Bundesanstalt PTB, Bundesallee 100, 38116 Braunschweig, Germany

ARTICLE INFO

Keywords:
Solar cell characterization
Short-circuit current
Linearity testing
Nonlinearity
White light response method
Differential spectral responsivity method
Spectral shaping
Differential responsivity
Spectral mismatch factor
AM1.5 spectrum
Grating light valve

ABSTRACT

This work presents a fast and accurate solar cell characterization method for determining the short-circuit current I_{STC} under standard test conditions. Additionally, the short-circuit current versus irradiance relation is derived, including accurately and precisely measured nonlinearities. Similar to the Differential Spectral Responsivity (DSR) method, our White Light Response (WLR) method uses a differential measurement technique with lock-in amplifiers. The first derivative of the short-circuit current versus irradiance relation (AM1.5-weighted differential responsivity) is measured at many irradiance levels without additional spectral mismatch corrections and considers the AM1.5 reference solar spectral irradiance distribution. The WLR method is significantly faster than the DSR method in determining the short-circuit current and nonlinearities. The highly spectrally nonlinear rear side of a bifacial PERC solar cell was investigated. The strong influence of the number of measured AM1.5-weighted differential responsivities and interpolation procedures on the short-circuit current I_{STC} is demonstrated. Finally, the accuracy of the results is discussed by means of a measurement comparison with the fully spectrally resolved DSR methods at PTB and CalLab PV Cells at ISE.

1. Introduction

The short-circuit current I_{STC} under Standard Test Conditions (STC) is of major interest in solar cell characterization. It is essential for performance evaluation, efficiency calculation, and calibration of a solar cell. Furthermore, an assumed uncertainty of 1% for the short-circuit current I_{STC} propagates to an uncertainty in the hundred million dollar range considering the yearly solar cell production and costs. Additionally, the linearity determination of the short-circuit current versus irradiance relation [1] is important especially for reference solar cells [2]. Thus, highly accurate methods for determining the short-circuit current I_{STC} and the linearity are in high demand.

Under STC, the solar cell must (i) have a temperature of 25 °C, (ii) be irradiated with the global AM1.5 reference solar spectral irradiance distribution (AM1.5 spectrum) [3,4] and (iii) at an irradiance of 1000 W/m^2. In indoor measurements, sun simulators try to reproduce the AM1.5 spectrum by combining and filtering radiation sources [5,6]. Even though the required irradiance can be achieved, a spectral mismatch is still present. A correction of the measured short-circuit current is applied to obtain the I_{STC} value [7] but an uncertainty remains.

A highly accurate procedure for determining I_{STC} and nonlinearities is the Differential Spectral Responsivity (DSR) method [8–12]. In this method, the absolute differential spectral responsivity $\tilde{s}_\lambda$ is measured. Afterwards, the AM1.5-weighted differential responsivity $\tilde{s}_{AM1.5}$ is calculated, which describes the slope of the short-circuit current versus irradiance curve. Then, an integration yields the short-circuit current I_{STC}. Thereby, the short-circuit current versus irradiance $I(E)$ curve is determined which allows for the detection of deviations in linearity [1]. However, the differential spectral responsivity $\tilde{s}_\lambda$ is determined by approximately 50 to 200 subsequently obtained values depending on its spectral resolution. Thus, it is a rather time-consuming procedure. Moreover, in nonlinear solar cell characterization the slope $\tilde{s}_{AM1.5}$ varies with the incident irradiance. Many measured $\tilde{s}_{AM1.5}$ data points at different irradiance levels are required to approximate the accurate slopes and, as a consequence, the accurate I_{STC}. Hence, the long measurement time is a serious limitation, which has led to some proposed simplifications [13–15].

To overcome these drawbacks, spectral shaping setups were built with a higher spectral resolution in an effort to reproduce the AM1.5 spectrum [16,17]. However, the generated irradiance was too low for large solar cells to fulfil STC. Work has been done to combine the advantages of the fast sun simulator approach with the accurate DSR method leading to the White Light Response (WLR) method [17,18]. Similar to the DSR method, a dual beam setup is used. One beam is

* Corresponding author.
E-mail address: matthias.muehleis@ise.fraunhofer.de (M. Mühleis).

https://doi.org/10.1016/j.solmat.2021.111208
Received 10 February 2021; Received in revised form 28 April 2021; Accepted 25 May 2021
Available online 1 June 2021

provided by steady bias lamps with a less demanding spectral irradiance distribution, generating a bias irradiance of up to 1000 W/m^2. As opposed to the DSR method, the other chopped beam is not monochromatic, but has a broadband radiation with the desired spectral irradiance distribution. In [17,18], a spectral mismatch to the AM1.5 spectrum was still present.

Recent developments led to a spectral shaping setup which is able to generate *chopped* radiation with a spectral distribution excellently matched to the AM1.5 spectrum [19]. In this work, we use this spectral shaping setup combined with the WLR method. We demonstrate that the spectral mismatch factors are negligible in measuring a spectrally nonlinear PERC solar cell which allows us to measure I_{STC} and nonlinearities quickly and accurately. Furthermore, this work shows the strong influence of the numerical integration method on the determined short-circuit current I_{STC} which has to be conducted in the WLR and DSR method. Finally, a measurement comparison between our new, fast, and accurate WLR setup and the DSR setups at PTB [20] and CalLab PV Cells at ISE [10] confirms the high accuracy of the determined short-circuit current I_{STC} and nonlinearities.

2. Theory

A solar cell generates the short-circuit current I_{E_λ}, when exposed to radiation with the spectral irradiance E_λ and irradiance $E := \int_0^\infty E_\lambda d\lambda$. Here, we investigate the AM1.5 spectrum, so $E_\lambda = E_\lambda^{AM1.5}$. The first derivative of the short-circuit current versus irradiance relation $I(E)$ at an irradiance level E_0 is the AM1.5-weighted differential responsivity of the solar cell [8]

$$\tilde{s}_{AM1.5}(E_0(I_{b,0})) = \frac{dI(E)}{dE}\Big|_{E=E_0(I_{b,0})} \approx \frac{\Delta I(E)}{\Delta E}\Big|_{E=E_0(I_{b,0})} \quad (1)$$

with the measured steady bias short-circuit current $I_{b,0}$. For nonlinear solar cells, the slope $\tilde{s}_{AM1.5}(E(I_b))$ depends on the irradiance $E(I_b)$ level of the incident radiation, which is in turn related to the generated I_b. Contrary to the irradiance E, the bias current I_b is a rather easily accessible quantity to be measured, and so $\tilde{s}_{AM1.5}(E(I_b))$ is written as a function of I_b. In the WLR method, the slope $\tilde{s}_{AM1.5}(I_{b,0})$ is experimentally approximated by the ratio of the small current response $\Delta I(E_0)$ to a small change of the irradiance ΔE with $\Delta E \ll E_0$ at an irradiance level $E_0(I_{b,0})$. The condition $\Delta E \ll E_0$ does not apply for very small bias irradiance E_0 levels. Yet there is a negligible impact on determining the short-circuit current at an irradiance $E_0 \gg \Delta E$. As the name implies, the AM1.5-weighted differential responsivity $\tilde{s}_{AM1.5}(I_b)$ can also be modelled as an integral of the differential *spectral* responsivity $\tilde{s}_\lambda(I_b)$ weighted with the AM1.5 spectrum [8]

$$\tilde{s}_{AM1.5}(I_{b,0}) = \frac{1}{E}\int_0^\infty \tilde{s}_\lambda(I_{b,0}) E_\lambda d\lambda \quad (2)$$

which is conducted in the DSR method. Cold mirror halogen lamps provide a spectral irradiance E_λ^b, which is sufficiently similar to the AM1.5 spectrum considering that the $\tilde{s}_\lambda(I_b)$ distribution remains almost unaffected by the difference between the bias and AM1.5 spectral distribution (i.e. $\tilde{s}_\lambda(I_b(E_\lambda^{AM1.5})) \approx \tilde{s}_\lambda(I_b(E_\lambda^b))$) [20]. Nevertheless, an additional measurement uncertainty of 0.1% (coverage factor [21] k = 2) is introduced [20] and is valid in the DSR and WLR method. Consequently, such broadband bias lamps with a less demanding spectral irradiance E_λ^b can be used to generate the steady bias currents I_b of the solar cell.

However, the small change of irradiance ΔE in Eq. (1) must exhibit the reference spectral irradiance ΔE_λ to get accurate results for the determined I_{E_λ} (here: $\Delta E_\lambda = \Delta E_\lambda^{AM1.5}$). A spectral mismatch between the generated ΔE_λ^{sim} and the reference $\Delta E_\lambda^{AM1.5}$ might change the differential short-circuit current response $\Delta I(E)$ in Eq. (1). It could be corrected with the spectral mismatch factor (SMM) [7]

$$SMM = \frac{\int \Delta E_\lambda^{AM1.5} \tilde{s}_\lambda^{RC}(I_{b,rc}) d\lambda \int \Delta E_\lambda^{sim} \tilde{s}_\lambda^{TC}(I_b) d\lambda}{\int \Delta E_\lambda^{sim} \tilde{s}_\lambda^{RC}(I_{b,rc}) d\lambda \int \Delta E_\lambda^{AM1.5} \tilde{s}_\lambda^{TC}(I_b) d\lambda} \quad (3)$$

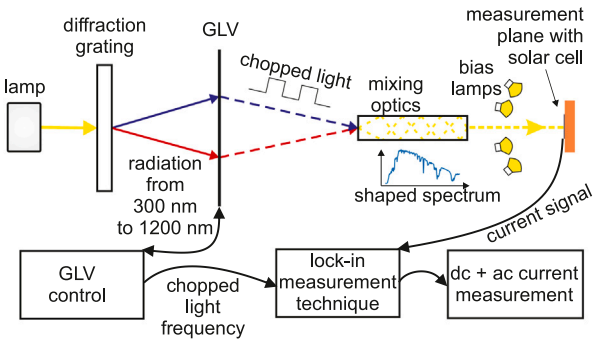

Fig. 1. Schematic drawing of the experimental setup for fast and accurate linearity measurements and short-circuit current I_{STC} determination of solar cells. The optical setup reproduces a relative spectral irradiance distribution equivalent to the AM1.5 spectrum. The AM1.5-weighted differential responsivity $\tilde{s}_{AM1.5}(I_b)$ and the bias short-circuit current I_b, generated by the bias lamps, are measured.

with the differential spectral responsivity $\tilde{s}_\lambda^{TC}(I_b)$ of the test solar cell at the bias current I_b and the differential spectral responsivity $\tilde{s}_\lambda^{RC}(I_{b,rc})$ of the calibrated reference solar cell at the bias current $I_{b,rc}$.

Finally, the irradiance E is written as a function of the bias current I_b and with Eq. (1), we follow that

$$E = \int_0^{I_b=I_{E_\lambda}} \frac{dE(I_b)}{dI} dI_b = \int_0^{I_b=I_{E_\lambda}} \frac{1}{\tilde{s}_{AM1.5}(I_b)} dI_b. \quad (4)$$

The short-circuit current I_{STC} under STC is then determined by a numerical approximation of the upper limit of the integral by approaching E_{STC} = 1000 W/m^2. Thereby, the short-circuit current versus irradiance relation $I(E)$ is derived. Deviations from an assumed linear relation are quantified with the linearity factor R [1]

$$R(E) = \frac{I(E)}{E}\frac{E_{STC}}{I_{STC}} \quad (5)$$

which is by definition $R(E_{STC}) = 1$ for the irradiance E_{STC}.

3. Experimental setup

The broadband radiation from a lamp was diffracted by a grating and was focused wavelength-dependent on a Grating Light Valve (GLV) from Silicon Light Machines as shown in Fig. 1. The GLV is a spatial light modulator [22,23] and was used to adjust the spectral irradiance in the wavelength range from 355 nm to 1200 nm with a spectral resolution of approximately 7 nm to 15 nm. A further beneficial feature of the GLV is its capability to generate a pulsed radiation with a precise frequency f_0 adjustable from 30.8 mHz up to 13.5 kHz (in this work: f_0 = 133 Hz). Mixing optics merged all wavelengths. The uniformly irradiated area in the measurement plane had a size of 7 cm × 7 cm. The spectral shaping part of the setup is described in detail in [19].

Fig. 2 shows the spectral irradiance ΔE_λ^{sim} (superscript indicates the solar simulator) of the chopped radiation which has been adapted to the slightly smoothed AM1.5 spectrum $E_\lambda^{AM1.5,3nm}$ at an irradiance level of approximately 0.1 W/m^2. In the WLR method, the irradiance of the chopped radiation must be as low as possible (Eq. (1)). ΔE_λ^{sim} was measured with a high-quality CCD multi-channel spectrometer from Zeiss which was calibrated with a standard lamp from PTB. The spectrometer has a spectral resolution of approximately 3 nm. Consequently, we have chosen the slightly smoothed AM1.5 spectrum as a target to achieve the lowest uncertainty in the spectral mismatch factor (Section 4.1 and [17]). The smoothed AM1.5 spectrum was generated by a convolution of the AM1.5 spectrum and a Gaussian function with a full width at half maximum of 3 nm. An excellent spectral match between ΔE_λ^{sim} and the smoothed AM1.5 spectrum was achieved. Remaining deviations were mostly smaller than the spectral measurement noise, which was between 0.5% and 3.0% [19]. A slightly increased spectral irradiance

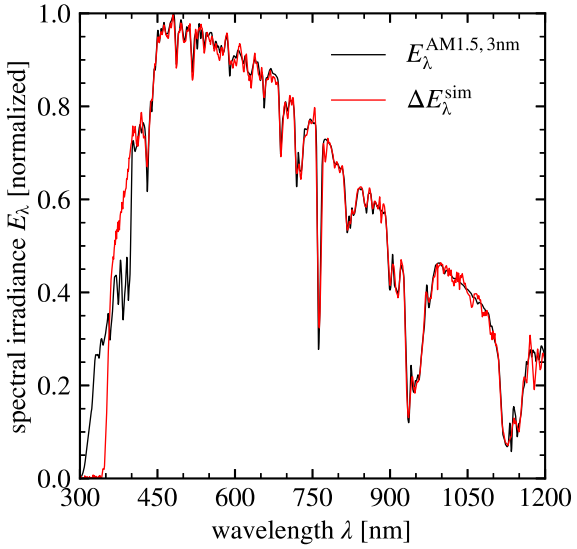

Fig. 2. Spectral irradiance $\Delta E_\lambda^{\mathrm{sim}}$ of the generated chopped radiation and the slightly smoothed AM1.5 spectrum. An excellent spectral match is achieved. The lack of irradiance below 355 nm is compensated by a higher spectral irradiance between 355 nm and 400 nm.

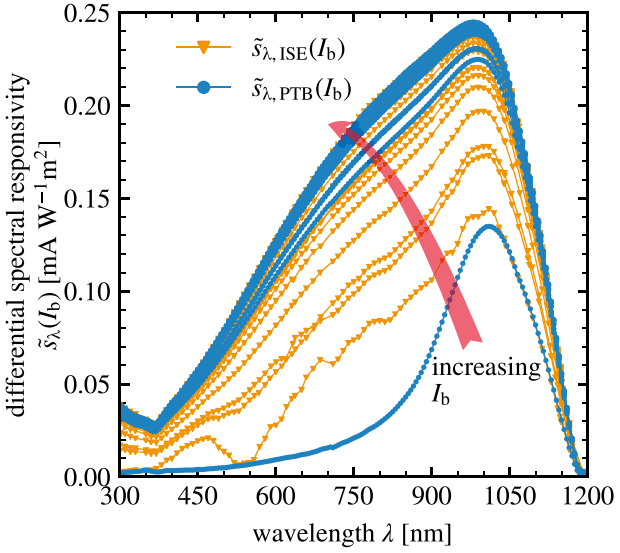

Fig. 3. Differential spectral responsivities $\tilde{s}_\lambda(I_\mathrm{b})$ for different bias currents I_b measured at ISE and PTB. The solar cell is spectrally nonlinear.

between 355 nm and 400 nm compensated for the lack of radiation below 355 nm. A detailed analysis of the spectral uncertainties has been conducted at the CalLab PV Cells at ISE. The spectral uncertainties were propagated to the uncertainty of the short-circuit current I_{STC}.

The experimental setup (Fig. 1) is equipped with cold mirror halogen lamps which irradiated the solar cell with a bias irradiance E^b adjustable to over 1000 W/m^2 and generated a steady bias current I_b signal. The solar cell was kept under short-circuit condition with a transimpedance amplifier developed in-house. The terminal voltage and the steady bias current I_b of the solar cell were tracked by digital multimeters (34461A/Keysight). The solar cell was kept at the temperature of 25.0 °C which was measured at the front of the solar cell using a tactile sensor. Due to the incident pulsed radiation, the solar cell responded with a pulsed current signal ΔI_{f_0} with the frequency f_0. The pulsed component ΔI_{f_0} was precisely recovered with a lock-in amplifier (7265/ametek) within a few seconds of generating the signal V. The lock-in amplifier received the required reference frequency f_0 from the GLV control. Prior to the test cell measurement, a WPVS reference solar cell [24] calibrated at PTB was measured at one bias current $I_\mathrm{b}^{\mathrm{RC}}$ generating the signal $V^{\mathrm{RC}}(I_\mathrm{b}^{\mathrm{RC}})$. Using the corresponding $\tilde{s}_{\mathrm{AM1.5}}^{\mathrm{RC}}(I_\mathrm{b}^{\mathrm{RC}})$ data point provided by PTB (which was calculated with Eq. (2) from a measured differential spectral responsivity $\tilde{s}_\lambda(I_\mathrm{b}^{\mathrm{RC}})$ at PTB) enabled us to determine the *absolute* AM1.5-weighted differential responsivities $\tilde{s}_{\mathrm{AM1.5}}(I_\mathrm{b})$ of the test solar cell with the measured lock-in signals $V^{\mathrm{TC}}(I_\mathrm{b})$ at arbitrarily chosen, adjustable bias irradiance E^b levels with

$$\tilde{s}_{\mathrm{AM1.5}}(I_\mathrm{b}) = \tilde{s}_{\mathrm{AM1.5}}^{\mathrm{RC}}(I_\mathrm{b}^{\mathrm{RC}}) \frac{V^{\mathrm{TC}}(I_\mathrm{b})}{V^{\mathrm{RC}}(I_\mathrm{b}^{\mathrm{RC}})} \frac{1}{\mathrm{SMM}}. \tag{6}$$

A spectral mismatch correction could be conducted with the SMM factors (Eq. (3)) but was not necessary in this work (Section 4.1). The short-circuit current versus irradiance relation of the reference solar cell was not required. There are plans to install a monitor cell in the future. In this case, its absence is taken into account by an additional introduced uncertainty of 0.2% ($k = 2$).

For validation of this setup, a measurement comparison with the DSR setups at PTB and ISE was performed. The test solar cell was chosen as a passivated-emitter-and-rear cell (PERC) with a silicon oxynitride/silicon nitride rear passivation [25]. The rear side of the solar cell was highly spectrally nonlinear due to inversion layer shunting [26,27] and was investigated in this work. The uncertainty in the WLR setup due to a spatially non-uniform irradiation was approximately 0.2% ($k = 2$) considering the different sizes of the test solar cell of 5.12 cm^2 and the reference solar cell of 4 cm^2.

In the DSR method, the differential spectral responsivity $\tilde{s}_\lambda(I_\mathrm{b})$ is determined similarly to Eq. (1) by means of measuring the current response to a chopped monochromatic radiation (instead of broadband radiation in the WLR method) with lock-in amplifiers. In case of nonlinear solar cells, it is conducted at different levels of steady bias currents I_b generated by bias lamps. The DSR measurement at PTB was conducted as a primary method. A $\tilde{s}_\lambda$ curve was measured between the wavelengths 280 nm and 1200 nm with a resolution of 5 nm. The DSR measurement at ISE was conducted as a secondary method with a reference solar cell calibrated at PTB and with a wavelength resolution of 10 nm. A further description of the DSR setup at PTB and ISE is found in [20] and [10] respectively. One data point at a wavelength λ in the $\tilde{s}_\lambda$ curve had a similar measurement time as the $\tilde{s}_{\mathrm{AM1.5}}$ data point in the WLR setup. Hence, the WLR setup was significantly faster in determining the AM1.5-weighted differential responsivity $\tilde{s}_{\mathrm{AM1.5}}$ than the DSR setup.

4. Results and discussion

4.1. Differential spectral responsivities and spectral mismatch factors

Fig. 3 shows the differential spectral responsivities $\tilde{s}_\lambda(I_\mathrm{b})$ at different bias currents I_b determined with the DSR setup at PTB [20] and CalLab PV Cells at ISE [10]. The relative distribution of $\tilde{s}_\lambda(I_\mathrm{b})$ changes and their absolute values increase with increasing bias currents I_b. Due to this high spectral nonlinearity, the solar cell is an excellent test device to evaluate the accuracy of a characterization method and is considered as a case example for linearity testing of photovoltaic devices. The lowest $\tilde{s}_{\lambda,\mathrm{ISE}}(I_{\mathrm{b,min}})$ distribution obtained at ISE showed an additional effect due to the significant contribution of the monochromatic radiation to the steady bias current $I_{\mathrm{b,min}}$. Because the values in the $\tilde{s}_\lambda(I_\mathrm{b})$ distribution increase with rising bias current, the $\tilde{s}_{\lambda,\mathrm{ISE}}(I_{\mathrm{b,min}})$ distribution reflects the spectrally dependent irradiance of the monochromatic radiation. We considered this by an additional measurement uncertainty at very low irradiance values.

Next, the spectral mismatch factors (SMM) were calculated with Eq. (3) using either the $\tilde{s}_\lambda(I_\mathrm{b})$ data from ISE or from PTB. The uncertainties of SMM were determined using the Monte-Carlo method [21]. Here,

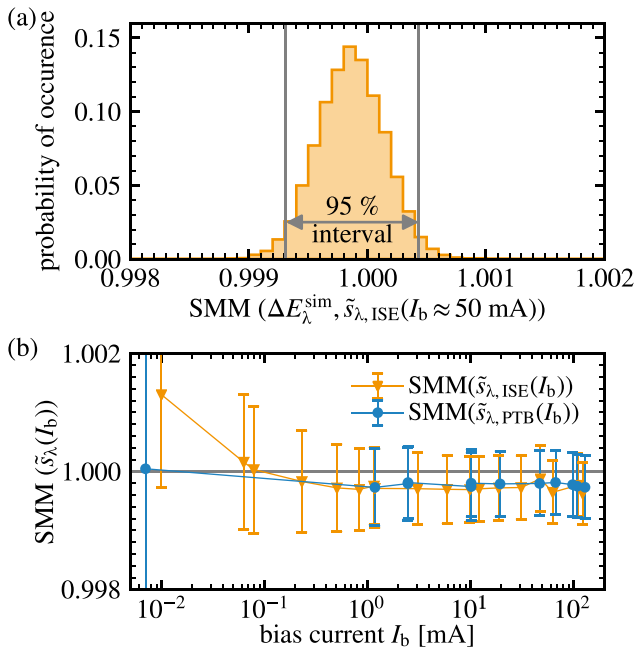

Fig. 4. Spectral mismatch factors (SMM) and their uncertainties for the measured ΔE_λ^{sim} spectrum and the differential spectral responsivities $\tilde{s}_\lambda(I_b)$. (a) Example for a distribution of SMM values generated with the Monte-Carlo method. The probabilistically symmetric 95% coverage interval of the distribution determines the uncertainty of SMM. (b) The SMM values are close to unity for all $\tilde{s}_\lambda(I_b)$ curves measured at CalLab PV Cells at ISE and PTB due to the excellent spectral match of the ΔE_λ^{sim} spectrum to the AM1.5 spectrum. (For interpretation of the references to colour in this figure legend, the reader is referred to the web version of this article.)

the idea is to slightly change the input parameters of SMM by means of a random sampling from probability distributions, which represent the individual uncertainty contributions. Thus, the distributions of the input parameters of SMM are propagated to the SMM distribution. The random sampling is conducted many times (approximately 10^4–10^5) resulting in a SMM distribution which is shown in Fig. 4(a). The length of the probabilistically symmetric 95% coverage interval defines the uncertainty of SMM. In the present case, the distribution is well described by a normal probability distribution and its twofold standard deviation ($k = 2$) is equal to the 95% coverage interval.

The SMM for ΔE_λ^{sim} and the varying differential spectral responsivities $\tilde{s}_{\lambda,ISE}(I_b)$ and $\tilde{s}_{\lambda,PTB}(I_b)$ lie with a probability of 95% between approximately 0.999 and 1.001 as indicated by the orange and blue error bars in Fig. 4(b). A further reduction of the uncertainty of SMM would require a significant improvement in the spectral measurements. The smoothed AM1.5 spectrum, which we used as the target reference spectral irradiance E_λ^{ref} (Fig. 2), would result in the lowest uncertainty of SMM. Due to the bandwidth and wavelength accuracy of the spectrometer, it is beneficial to slightly smooth the sharp features in the AM1.5 spectrum.

We emphasize that a chopped radiation with other spectral irradiance distributions generated from state-of-the-art sun simulators (LED, xenon arc lamp) combined with the varying spectral responsivities would require significant spectral mismatch corrections.

As a result, a spectral mismatch correction is negligible in our setup and is instead considered as a minor uncertainty contribution of approximately 0.1% ($k = 2$) in this extreme case scenario. Thus, an AM1.5-weighted differential responsivity is directly measured within a few seconds. Differential *spectral* responsivities are not necessary, which drastically reduces the measurement time of this WLR setup compared to a DSR setup.

4.2. Influence of numerical integration methods on the short-circuit current determination

In the DSR method and in our new WLR method, the short-circuit current I_{STC} is calculated by using Eq. (4). The integration, which is included, is conducted numerically after the AM1.5-weighted differential responsivities $\tilde{s}_{AM1.5}(I_b)$ at the different bias currents I_b are determined.

Fig. 5(a) shows $\tilde{s}_{AM1.5}$ of the test solar cell measured with our new WLR setup at 25 different bias currents I_b. Especially at low bias currents I_b, a strong increase in $\tilde{s}_{AM1.5}$ was observed showing the strong nonlinearity of the solar cell. The inset depicts the data on a logarithmic I_b-scale. Here, the curve appears more linearly, which shows that $\tilde{s}_{AM1.5}$ increases almost logarithmically.

According to Eq. (4), the inverse AM1.5-weighted differential responsivities $1/\tilde{s}_{AM1.5}(I_b)$ are integrated until the irradiance $E_{STC} = 1000\,W/m^2$ is achieved and the upper limit determines the short-circuit current I_{STC}, which is illustrated as the red area and arrow in Fig. 5(b). As a result, the short-circuit current to irradiance relation is derived (Fig. 5(c)).

The influence of two different numerical integration methods is illustrated in the case that 5 measured $\tilde{s}_{AM1.5}(I_b)$ data points are available. A probably easily implementable method is to integrate $1/\tilde{s}_{AM1.5}(I_b)$ with the trapezoidal rule. It is equivalent to a linear piecewise interpolation between $1/\tilde{s}_{AM1.5}(I_b)$ and a consecutive calculation of the underlying area represented by the purple connecting lines in Fig. 5(b). Due to the nonlinear $1/\tilde{s}_{AM1.5}(I_b)$ curve, the calculated area (and so the irradiance) is larger and the determined short-circuit current I'_{STC} is smaller (purple area and arrow in Fig. 5(b)).

The other integration method uses a logarithmic piecewise interpolation between $\tilde{s}_{AM1.5}(I_b)$, which is a linear interpolation in the logarithmic space represented by the connecting lines in the inset in Fig. 5(a). It is superior to the linear interpolation due to the rather logarithmic increase of $\tilde{s}_{AM1.5}(I_b)$. The resulting $1/\tilde{s}_{AM1.5}(I_b)$ curve is closer to the true curve and its underlying area reduces overestimation of the true area (blue curve and area in Fig. 5(b)). A logarithmic extrapolation towards the bias currents $I_b = 0\,mA$ is not feasible (or an offset has to be assumed). Here, we advise a linear extrapolation or using $\tilde{s}_{AM1.5}(I_{b,min})$ of the minimal $I_{b,min}$ twice.

In the case of the large number of 25 measured $\tilde{s}_{AM1.5}(I_b)$, the resulting short-circuit currents I_{STC} deviate with only −0.04%, if we use the different interpolation methods as specified in Table 1. However, if the number of measured $\tilde{s}_{AM1.5}(I_b)$ data points is limited, for example due to a limited measurement time, the influence of the interpolation procedure increases.

Furthermore, the distribution of the bias currents I_b, where $\tilde{s}_{AM1.5}(I_b)$ is measured, must be carefully chosen. One possibility is an equally spaced distribution, illustrated as green crosses in Fig. 5(a), assuming 5 available $\tilde{s}_{AM1.5}(I_b)$ data points. Another possibility is a logarithmically spaced distribution shown as blue stars.

The largest deviation to the most accurate short-circuit current $I_{STC} = 113.95\,mA$ is observed with −5.76% at 5 measured $\tilde{s}_{AM1.5}(I_b)$ with equally spaced bias currents I_b and linearly interpolated $1/\tilde{s}_{AM1.5}(I_b)$ as specified in Table 1. The deviation drastically decreases to −0.10%, if 8 measured $\tilde{s}_{AM1.5}(I_b)$ with logarithmically spaced I_b are available and a logarithmic interpolation is conducted. Nevertheless, even a deviation of −0.10% is relevant in highly accurate solar cell characterization. Furthermore, a different distribution than the logarithmically spaced I_b could result in a higher deviation. For instance, equally spaced I_b yield a deviation of −0.43%.

Even though the logarithmic interpolation could compensate for the limited number of measured $\tilde{s}_{AM1.5}(I_b)$ to a certain extent, it is not obvious prior to a solar cell characterization if the logarithmic interpolation offers acceptable results for every device under test. A nonlinearity can originate for various reasons and different irradiance dependent nonlinearities were observed [2,12,28,29]. We believe that finding a physical law for a justified fitting procedure is hardly feasible.

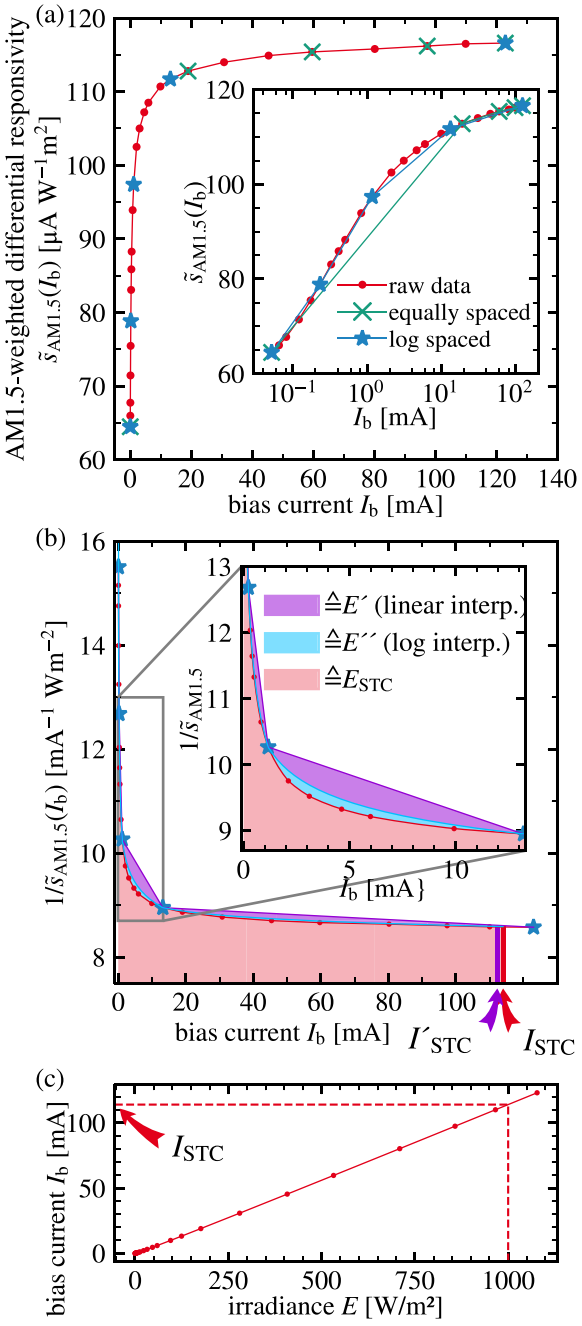

Fig. 5. Influence of the number of measured AM1.5-weighted differential responsivities $\tilde{s}_{AM1.5}(I_b)$ and interpolation procedures on the short-circuit current I_{STC}. (a) $\tilde{s}_{AM1.5}(I_b)$ on a logarithmic I_b-axis appears more linearly. Thus a logarithmic interpolation and equally logarithmic spaced $\tilde{s}_{AM1.5}(I_b)$ should be used (blue lines and stars). (b) The area under the $1/\tilde{s}_{AM1.5}$ curve (red coloured) for $0 \le I_b \le I_{STC}$ corresponds to the irradiance $E_{STC} = 1000\,W/m^2$. The calculated I_{STC} is faulty when too few $\tilde{s}_{AM1.5}(I_b)$ are measured (purple arrow). A logarithmic interpolation in $\tilde{s}_{AM1.5}(I_b)$ (blue line) is superior to a linear interpolation in $1/\tilde{s}_{AM1.5}(I_b)$ (purple line). (c) Derived short-circuit current versus irradiance relation. (For interpretation of the references to colour in this figure legend, the reader is referred to the web version of this article.)

Thus, a sufficiently large quantity of measured $\tilde{s}_{AM1.5}(I_b)$ is preferred resulting in a short-circuit current I_{STC} which is robust against the chosen interpolation procedure. As demonstrated by the 25 $\tilde{s}_{AM1.5}(I_b)$ values, measured with our new WLR setup, the dependence due to the numerical integration procedure is almost negligible.

Additionally, we investigated the propagation of an uncorrelated uncertainty in the AM1.5-weighted differential responsivities $\tilde{s}_{AM1.5}(I_b)$

Table 1
Calculated short-circuit current I_{STC} for different quantities and bias current I_b intervals of measured $\tilde{s}_{AM1.5}(I_b)$ and for different $\tilde{s}_{AM1.5}$-interpolation procedures. Absolute I_{STC}, relative uncertainty of I_{STC} for an assumed 1% uncorrelated uncertainty of $\tilde{s}_{AM1.5}$ ($k = 2$), and relative deviation to the most accurate $I_{STC} = 113.95\,mA$ are tabulated. Green rectangles highlight the most accurate result and the results with rather small deviations. A logarithmic interpolation between the measured $\tilde{s}_{AM1.5}(I_b)$ and a high quantity of measured $\tilde{s}_{AM1.5}(I_b)$ provides the highest accuracy.

Number of measured $\tilde{s}_{AM1.5}(I_b)$	I_{STC} [mA]			
	$1/\tilde{s}_{AM1.5}(I_b)$ linearly interpolated		$\tilde{s}_{AM1.5}(I_b)$ logarithmically interpolated	
	I_b equally spaced	I_b log spaced	I_b equally spaced	I_b log spaced
5	107.39 ±0.56% (−5.76%)	112.29[a] ±0.69% (−1.46%)	113.18 ±0.57% (−0.68%)	113.56[a] ±0.70% (−0.34%)
8	109.61 ±0.40% (−3.81%)	113.44 ±0.63% (−0.45%)	113.46 ±0.40% (−0.43%)	113.84 ±0.60% (−0.10%)
25 (all)	113.90 ±0.34% (−0.04%)		113.95[a] ±0.34% (0.00%)	

[a]Illustrated in Fig. 5(b).

(for instance the uncertainty due to the measurement repeatability) to the uncertainty of the short-circuit current $U(I_{STC})$. Again, the Monte-Carlo method was used [21]. For illustration purposes, we assumed an uncertainty of 1% ($k = 2$). The resulting uncertainties $U(I_{STC})$ ($k = 2$) are also specified in Table 1. First, an increasing number of measured $\tilde{s}_{AM1.5}(I_b)$ decreases the uncertainty $U(I_{STC})$. Secondly, the interpolation procedure has a negligible effect on $U(I_{STC})$. However, equally spaced I_b intervals lead to lower $U(I_{STC})$ than logarithmically spaced I_b intervals. This is in contrast to the trend of the increasing deviations in I_{STC} due to the integration error. In the logarithmically spaced I_b values, the last two $\tilde{s}_{AM1.5}(I_b)$ data points include a large I_b interval and mainly contribute to I_{STC}, which is in turn also valid for their uncertainties.

Hence, we strongly advice logarithmically spaced bias currents I_b for low I_b values to reduce numerical integration errors. However, equally spaced bias currents I_b are preferred for large I_b values to reduce the contribution of uncorrelated uncertainties in $\tilde{s}_{AM1.5}(I_b)$ to the short-circuit current I_{STC}. This is considered in the 25 measured $\tilde{s}_{AM1.5}(I_b)$ which provide an accurate and precise I_{STC}.

4.3. Determined short-circuit current with the WLR method and DSR methods

We evaluated the measured AM1.5-weighted differential responsivities $\tilde{s}_{AM1.5}(I_b)$ and the resulting short-circuit current I_{STC} by a measurement comparison with the fully spectrally resolved DSR method at PTB and CalLab PV Cells at ISE.

Fig. 6 shows the AM1.5-weighted differential responsivities $\tilde{s}_{AM1.5}(I_b)$ measured with our new WLR method and calculated from the differential spectral responsivities (Fig. 3 and Eq. (2)). The relative deviations ($\Delta\tilde{s} = \tilde{s}_x/\tilde{s}_y - 1$) are within their uncertainties close to zero and are shown in Fig. 6(b). The deviations are mostly smaller than approximately 0.5%. For very small bias currents I_b, the deviations and their uncertainties slightly increase mainly due to the large slope in the $\tilde{s}_{AM1.5}(I_b)$ curve. The measurement comparison with the DSR setup at ISE was conducted with the same calibrated reference solar cell which had an assigned uncertainty of approximately 0.4% ($k = 2$). Furthermore, some measurement devices were used twice. Hence, the

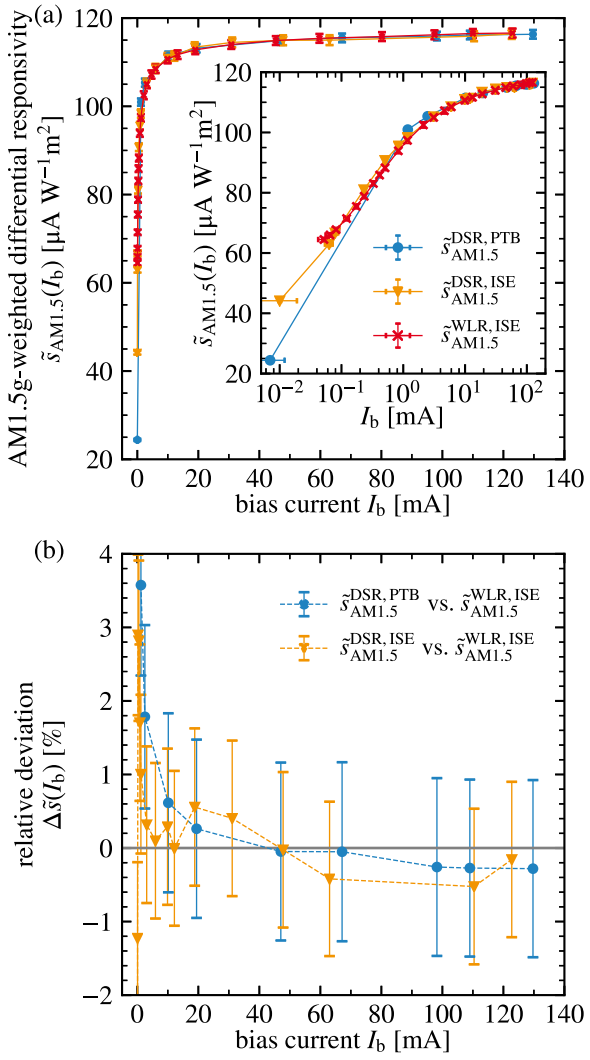

Fig. 6. AM1.5-weighted differential responsivities $\tilde{s}_{AM1.5}(I_b)$ and their relative differences. (a) $\tilde{s}_{AM1.5}(I_b)$ is highly dependent on the bias current I_b. (b) The relative differences $\Delta\tilde{s}(I_b)$ are within their uncertainties close to zero verifying the excellent ability of the WLR method to measure $\tilde{s}_{AM1.5}(I_b)$ data points.

results are correlated. This is considered in the assigned uncertainties of their relative deviations. The measurement comparison with PTB is less correlated. The connected calibration chain over the same reference detector used at PTB yields a correlation of 0.1% ($k = 2$). Therefore, the uncertainties of the relative deviations are slightly greater.

Table 2 presents the resulting short-circuit currents I_{STC} under STC calculated with Eq. (4). Additionally, a second measurement, carried out with the WLR setup and the DSR setup at PTB, yielded $I_{STC}^{PTB,2} = (114.25 \pm 0.91)\,mA$ ($k = 2$) and $I_{STC}^{WLR,2} = (114.11 \pm 0.87)\,mA$ ($k = 2$). Due to the smaller number of measured $\tilde{s}_{AM1.5}(I_b)$ values in the DSR setups at PTB and ISE, the numerical integration was performed by using a logarithmic interpolation between the determined AM1.5-weighted differential responsivities $\tilde{s}_{AM1.5}(I_b)$ to decrease integration errors according to Section 4.2. In our new WLR setup, a linear interpolation is also feasible due to the larger number of measured $\tilde{s}_{AM1.5}(I_b)$ data points. The maximal relative deviation between the I_{STC} values and its uncertainty is $(0.4 \pm 1.1)\,\%$ ($I_{STC}^{PTB,2}/I_{STC}^{DSR,ISE} - 1$). It indicates the excellent agreement of the results because it encloses zero within its uncertainty. The assigned uncertainties were determined with the Monte-Carlo method [21] and considered a comprehensive uncertainty budget. The uncertainties of I_{STC} are approximately 0.8% ($k = 2$) and

Table 2
Short-circuit currents I_{STC} under STC with uncertainties ($k = 2$) determined with the different methods. All results match within their uncertainties, if a logarithmic interpolation is conducted between the measured $\tilde{s}_{AM1.5}(I_b)$ data points (dark green) proving the high accuracy of our new WLR^{ISE} setup. A linear interpolation is also feasible for the WLR^{ISE} method due to the high quantity of measured $\tilde{s}_{AM1.5}(I_b)$ data points (light green).

Method	WLR^{ISE}		DSR^{ISE}	DSR^{PTB}
inter-polation	Linear	log	log	log
I_{STC} [mA]	113.90 ±0.89	113.95 ±0.87	113.79 ±0.84	113.93 ±0.91

are quite similar for all setups. Note that for a linear cell, the assigned uncertainties of I_{STC} could be significantly lower.

The WLR method presented in this work requires a reference solar cell. Thus, it is stated as a secondary calibration method for determining the I_{STC} value. It introduces an additional measurement uncertainty compared to the DSR method at PTB which is used as a primary method. For the investigated test solar cell, however, measurement uncertainties arise from the strongly increasing $\tilde{s}_{AM1.5}(I_b)$ curve and the influence of the number of $\tilde{s}_{AM1.5}(I_b)$ data points. Consequently, the assigned uncertainties of the I_{STC} values are slightly smaller for the WLR method, which benefits from the larger number of measured $\tilde{s}_{AM1.5}(I_b)$ data points, in comparison with the DSR method at PTB.

4.4. Linearity factors

The linearity factors $R(E)$ calculated with Eq. (5) quantify the deviations of the determined short-circuit current versus irradiance relation $I(E)$ (Fig. 5(c)) from an assumed linear relation $E\frac{I_{STC}}{E_{STC}}$ with the same short-circuit current I_{STC}. As can be seen in Fig. 7(a), both DSR methods and the WLR method are able to determine the rather strong nonlinearity of the test solar cell. For an irradiance below $E < 100\,W/m^2$ (see inset), the short-circuit current deviates more than 10% ($R < 0.9$) from linearity. The linearity factors can be determined at arbitrarily chosen, adjustable bias irradiance levels. However, a smooth $\tilde{s}_{AM1.5}(I_b)$ curve with a sufficiently large number of data points is mandatory (Section 4.2). The measured nonlinearity might be relevant in determining the energy yield of the solar cell considering that yearly solar irradiance values are widely distributed from zero to over $E = 1000\,W/m^2$ [30]. Low irradiance values are especially relevant if the *rear* side of a bifacial solar cell is investigated [31], as it was done in this work.

The relative deviations ($= R_{DSR}/R_{WLR} - 1$) of the linearity factors $R(E)$ determined with the DSR setups and the WLR setup tend to decrease with increasing irradiance and are in good agreement with their estimated uncertainties ($k = 2$) as shown in Fig. 7(b). A relative deviation of zero for the irradiance $E_{STC} = 1000\,W/m^2$ is obvious because the corresponding linearity factor $R(E_{STC}) = 1$ is unity by definition (Eq. (5)). The uncertainties of the $\tilde{s}_{AM1.5}(I_b)$ data points were propagated to the uncertainties of the linearity factors with the Monte-Carlo method [21] considering correlations between the $\tilde{s}_{AM1.5}(I_b)$ data points and uncertainties of the bias currents I_b.

A correlation is introduced between the short-circuit current $I(E)$ at an irradiance E and the short-circuit current I_{STC} at $E_{STC} = 1000\,W/m^2$ due to the successive calculation of the short-circuit currents in Eq. (4). As a result, uncertainties which influence all $\tilde{s}_{AM1.5}(I_b)$ data points as a constant factor (fully correlated, Pearson correlation coefficient $\rho = 1$) are almost negligible in determining the uncertainty of the linearity factor. These fully correlated uncertainties are transformed to uncertainties of the assigned irradiance E levels of the linearity factors $R(E)$ (error bars in direction of the irradiance E axis in Fig. 7(a) and (c)). The relative uncertainties of the linearity factors are much lower than the relative uncertainties of the short-circuit currents (Fig. 7(c) and Table 2) because most of the uncertainty components of the

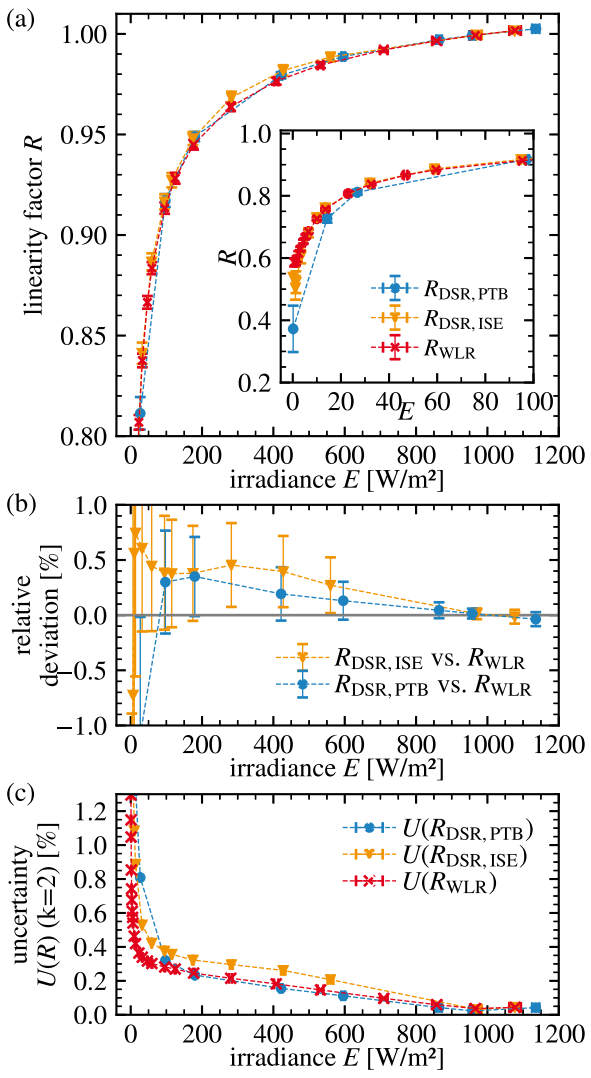

Fig. 7. Nonlinearity of the solar cell. (a) Linearity factors $R(E)$ indicate nonlinear short-circuit current versus irradiance $I(E)$ relation. (b) Relative deviations between the linearity factors determined with the DSR setups at PTB and CalLab PV Cells at ISE and the WLR setup. (c) Relative uncertainty of the linearity factors $U(R)$ decrease with increasing irradiance. (For interpretation of the references to colour in this figure legend, the reader is referred to the web version of this article.)

$\tilde{s}_{AM1.5}(I_b)$ data points are fully correlated (examples for the WLR setup: uncertainty of the $\tilde{s}^{RC}_{AM1.5}(I^{RC}_b)$ data point of the reference solar cell (Eq. (6)), uncertainty due to an imperfect positioning of the test and reference solar cell in the measurement plane, uncertainty due to a spatial non-uniformity of the radiation). Thus, the WLR method is negligibly dependent on the uncertainty of the reference solar cell in determining the linearity factors. This is similar to the behaviour of the N-lamp method which is also used for linearity measurements [1,2] and the DSR method [12].

Uncertainty components of the $\tilde{s}_{AM1.5}(I_b)$ data points which are uncorrelated ($\rho = 0$) influence the uncertainty of the linearity factor with each increasing $\tilde{s}_{AM1.5}(I_b)$ data point in a reduced way due to the successive calculation of the short-circuit currents and their introduced correlations in Eq. (5). Some effects might influence the $\tilde{s}_{AM1.5}(I_b)$ data points in a more continuous way, for example the change of the $\tilde{s}_{AM1.5}(I_b)$ data points due to deviations between the bias spectrum and the AM1.5 spectrum, deviations between the chopped ΔE_λ spectrum and the AM1.5 spectrum in the WLR method, or due to the absence of a monitor cell in the current WLR facility. We simulated these effects in the Monte-Carlo method by introducing correlations between the $\tilde{s}_{AM1.5}(I_b)$ data points ($0 < |\rho| < 1$). These correlated uncertainties mainly increase the uncertainties of the linearity factors in the middle range of the irradiance values. An underestimation of these correlated uncertainties could explain the slightly larger than expected relative deviations between the results determined with the WLR and DSR setups at ISE (orange in Fig. 7(b)). However, the influence of the spectral mismatch of ΔE_λ is investigated in detail in Section 4.1 and is almost negligible ($\leq 0.1\%$ ($k = 2$) for $\tilde{s}_{AM1.5}(I_b)$) in this extreme case scenario.

The uncertainties presented in Fig. 7 are specific for this measurement as they consider the shape of the $\tilde{s}_{AM1.5}(I_b)$ curve. For a linear solar cell, we expect lower uncertainties.

5. Conclusion and outlook

In this work, we have demonstrated a fast and highly accurate White Light Response (WLR) method which is able to determine nonlinearities and the short-circuit current I_{STC} of a solar cell under standard test conditions. Similar to the Differential Spectral Responsivity (DSR) method, a dual beam setup has been used. A developed spectral shaping setup was able to generate chopped radiation with a desired broadband spectral irradiance. Reproducing the relative distribution of the AM1.5 reference solar spectral irradiance enabled us to directly measure the AM1.5-weighted differential responsivities at different irradiance levels which represent the first derivative of the short-circuit current versus irradiance relation. A spectrally nonlinear PERC solar cell was investigated and considered as an extreme case scenario in a measurement comparison between our new WLR setup and the DSR setups at PTB and CalLab PV Cells at ISE. A detailed analysis of the spectral irradiance of the generated chopped radiation combined with the different spectral responsivities demonstrated that a spectral mismatch correction was negligible, even with this highly spectrally nonlinear solar cell. Consequently, spectral responsivities were not required, which shortens the measurement time of the AM1.5-weighted differential responsivity to a few seconds. Additionally, we have shown that many AM1.5-weighted differential responsivities were required to approximate the accurate short-circuit current I_{STC} of the nonlinear PERC solar cell. Here, our fast and new WLR setup is important. Furthermore, we advise a logarithmic interpolation during the calculation of I_{STC}. An insufficient number of measured AM1.5-weighted differential responsivities and a linear interpolation would result in an underestimation of the short-circuit current I_{STC}, and so of the performance of the nonlinear PERC solar cell. Finally, the determined nonlinearities and short-circuit currents I_{STC} were consistent with all three setups and proofed the high accuracy of our new WLR setup.

Of course, our new setup is applicable to linear solar cells. Here, we expect lower uncertainties. Further measurements are planned to show the wide spectrum of applications.

CRediT authorship contribution statement

Matthias Mühleis: Conceptualization, Formal analysis, Investigation (Experiments at ISE), Writing, Visualization. **Ingo Kröger:** Investigation (Experiments at PTB), Validation. **Jochen Hohl-Ebinger:** Investigation (Experiments at ISE), Validation.

Declaration of competing interest

The authors declare that they have no known competing financial interests or personal relationships that could have appeared to influence the work reported in this paper.

Acknowledgements

We thank Michael Rauer for fruitful discussions. The suggestions from the anonymous reviewers were greatly appreciated.

References

[1] IEC 60904–10, Photovoltaic devices – Part 10: Methods of linear dependence and linearity measurements, 2020-09.

[2] H. Müllejans, E. Salis, Linearity of photovoltaic devices: quantitative assessment with N-lamp method, Meas. Sci. Technol. 30 (6) (2019) 065008.

[3] IEC 60904–3, Photovoltaic devices – Part 3: Measurement principles for terrestrial photovoltaic (PV) solar devices with reference spectral irradiance data, 2019-02.

[4] C.A. Gueymard, D. Myers, K. Emery, Proposed reference irradiance spectra for solar energy systems testing, Sol. Energy 73 (6) (2002) 443–467.

[5] V. Esen, Ş. Sağlam, B. Oral, Light sources of solar simulators for photovoltaic devices: A review, Renew. Sustain. Energy Rev. 77 (2017) 1240–1250, http://dx.doi.org/10.1016/j.rser.2017.03.062, URL: http://www.sciencedirect.com/science/article/pii/S1364032117303787.

[6] M. Bliss, T.R. Betts, R. Gottschalg, An LED-based photovoltaic measurement system with variable spectrum and flash speed, Sol. Energy Mater. Sol. Cells 93 (6–7) (2009) 825–830.

[7] IEC 60904–7, Photovoltaic devices – Part 7: Computation of the spectral mismatch correction for measurements of photovoltaic devices, 2019-08.

[8] J. Metzdorf, Calibration of solar cells. 1: The differential spectral responsivity method, Appl. Opt. 26 (9) (1987) 1701–1708.

[9] S. Winter, T. Fey, I. Kröger, D. Friedrich, K. Ladner, B. Ortel, S. Pendsa, F. Witt, Design, realization and uncertainty analysis of a laser-based primary calibration facility for solar cells at PTB, Measurement 51 (2014) 457–463.

[10] M. Mundus, Ultrashort Laser Pulses for Electrical Characterization of Solar Cells, BoD–Books on Demand, 2016.

[11] D. Hinken, I. Kröger, S. Winter, R. Brendel, K. Bothe, Determining the spectral responsivity of solar cells under standard test conditions, Meas. Sci. Technol. 30 (12) (2019) 125008.

[12] M. Bliss, T. Betts, R. Gottschalg, E. Salis, H. Müllejans, S. Winter, I. Kroeger, K. Bothe, D. Hinken, J. Hohl-Ebinger, Interlaboratory comparison of short-circuit current versus irradiance linearity measurements of photovoltaic devices, Sol. Energy 182 (2019) 256–263.

[13] K. Bothe, D. Hinken, B. Min, C. Schinke, Accuracy of simplifications for spectral responsivity measurements of solar cells, IEEE J. Photovolt. 8 (2) (2018) 611–620.

[14] M. Bliss, A. Smith, T.R. Betts, J. Baker, F. de Rossi, S. Bai, T. Watson, H. Snaith, R. Gottschalg, Spectral response measurements of perovskite solar cells, IEEE J. Photovolt. 9 (1) (2018) 220–226.

[15] D.J. Wehenkel, K.H. Hendriks, M.M. Wienk, R.A.J. Janssen, The effect of bias light on the spectral responsivity of organic solar cells, Org. Electron. 13 (12) (2012) 3284–3290.

[16] T. Dennis, C. Yasanayake, T. Gerke, A. Payne, L. Eng, B. Fisher, M. Meitl, A programmable solar simulator for realistic seasonal, diurnal, and air-mass testing of multi-junction concentrator photovoltaics, in: I.P.S. Conference (Ed.), 2016 IEEE 43rd Photovoltaic Specialists Conference (PVSC), IEEE, [Piscataway, NJ], 2016, pp. 2327–2332, http://dx.doi.org/10.1109/PVSC.2016.7750054.

[17] M. Mundus, M. Kumar Dasa, X. Wang, J. Hohl-Ebinger, W. Warta, Spectrally shaped supercontinuum for advanced solar cell characterization, in: 31st EU PVSEC, 2015, pp. 514–519, http://dx.doi.org/10.4229/EUPVSEC20152015-2DO.4.6.

[18] J. Hohl-Ebinger, G. Siefer, W. Warta, Non-linearity of solar cells in spectral response measurements, in: 22nd EU PVSEC, 2007, pp. 422–424.

[19] M. Mühleis, J. Hohl-Ebinger, Programmable spectral shaping demonstrated at the solar spectral irradiance distribution, Opt. Express 29 (6) (2021) 8223–8234, http://dx.doi.org/10.1364/OE.417790.

[20] I. Kröger, D. Friedrich, S. Winter, Calibration of solar cells beyond STC using the DSR method, in: IEEE 7th World Conference on Photovoltaic Energy Conversion (WCPEC)(A Joint Conference of 45th IEEE PVSC, 28th PVSEC & 34th EU PVSEC), IEEE, 2018, pp. 3492–3497.

[21] BIPM, IEC, IFCC, ILAC, ISO, IUPAC, IUPAP and OIML, Evaluation of measurement data — Supplement 1 to the "Guide to the expression of uncertainty in measurement" — Propagation of distributions using a Monte Carlo method, 2010.

[22] D.T. Amm, R.W. Corrigan, 5.2: Grating Light Valve™ Technology: Update and Novel Applications, in: SID Symposium Digest of Technical Papers, Wiley Online Library, 1998, pp. 29–32.

[23] D.T. Amm, R.W. Corrigan, Optical Performance of the Grating Light Valve Technology, in: Projection Displays V, International Society for Optics and Photonics, 1999, pp. 71–78.

[24] C.R. Osterwald, S. Anevsky, K. Bücher, A.K. Barua, P. Chaudhuri, J. Dubard, K. Emery, B. Hansen, D. King, J. Metzdorf, The world photovoltaic scale: an international reference cell calibration program, Prog. Photovolt., Res. Appl. 7 (4) (1999) 287–297.

[25] P. Palinginis, C. Kusterer, S. Steckemetz, R. Köhler, R. Härtwig, T. Weber, M. Müller, G. Fischer, H. Neuhaus, Pioneering the industrialization of PERC technology: A review of the development of mono-and bifacial PERC solar cells at solarworld, Photovolt. Int. 42 (2019) 51–72.

[26] M. Rauer, F. Guo, J. Hohl-Ebinger, Accurate measurement of bifacial solar cells with single- and both-sided illumination, in: 36th EU PVSEC, 2019, pp. 239–246, http://dx.doi.org/10.4229/EUPVSEC20192019-2CO.12.1.

[27] S. Dauwe, L. Mittelstädt, A. Metz, R. Hezel, Experimental evidence of parasitic shunting in silicon nitride rear surface passivated solar cells, Prog. Photovolt., Res. Appl. 10 (4) (2002) 271–278.

[28] M. Mundus, B. Venkataramanachar, R. Gehlhaar, M. Kohlstädt, B. Niesen, W. Qiu, J.P. Herterich, F. Sahli, M. Bräuninger, J. Werner, J. Hohl-Ebinger, G. Uytterhoeven, U. Würfel, C. Ballif, M.C. Schubert, W. Warta, S.W. Glunz, Spectrally resolved nonlinearity and temperature dependence of perovskite solar cells, Sol. Energy Mater. Sol. Cells 172 (2017) 66–73, http://dx.doi.org/10.1016/j.solmat.2017.07.013.

[29] B.H. Hamadani, A. Shore, J. Roller, H.W. Yoon, M. Campanelli, Non-linearity measurements of solar cells with an LED-based combinatorial flux addition method, Metrologia 53 (1) (2016) 76.

[30] D. Dirnberger, G. Blackburn, B. Müller, C. Reise, On the impact of solar spectral irradiance on the yield of different PV technologies, Sol. Energy Mater. Sol. Cells 132 (2015) 431–442.

[31] U.A. Yusufoglu, T.M. Pletzer, L.J. Koduvelikulathu, C. Comparotto, R. Kopecek, H. Kurz, Analysis of the annual performance of bifacial modules and optimization methods, IEEE J. Photovolt. 5 (1) (2015) 320–328, http://dx.doi.org/10.1109/JPHOTOV.2014.2364406.